Long-Circulating 15 nm Micelles Based on Amphiphilic 3-Helix Peptide–PEG Conjugates

He Dong,[†] Nikhil Dube,[†] Jessica Y. Shu,[†] Jai W. Seo,[‡] Lisa M. Mahakian,[‡] Katherine W. Ferrara,[‡] and Ting Xu[†,§,⊥,*]

[†]Department of Materials Science & Engineering, University of California, Berkeley, California 94720, United States, [‡]Department of Biomedical Engineering, University of California, Davis, California 95616, United States, [§]Department of Chemistry, University of California, Berkeley, California 94720, United States, and [⊥]Materials Sciences Division, Lawrence Berkeley National Laboratory, Berkeley, California 94720, United States

ABSTRACT

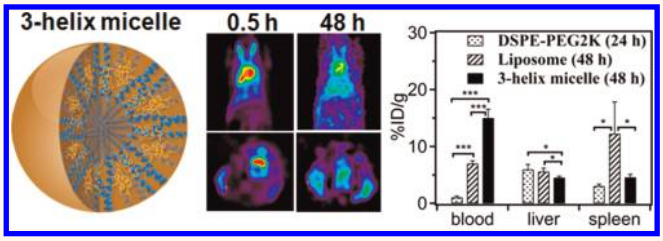

Generating stable, multifunctional organic nanocarriers will have a significant impact on drug formulation. However, it remains a significant challenge to generate organic nanocarriers with a long circulation half-life, effective tumor penetration, and efficient clearance of metabolites. We have advanced this goal by designing a new family of amphiphiles based on coiled-coil 3-helix bundle forming peptide–poly(ethylene glycol) conjugates. The amphiphiles self-assemble into monodisperse micellar nanoparticles, 15 nm in diameter. Using the 3-helix micelles, a drug loading of ~8 wt % was obtained using doxorubicin and the micelles showed minimal cargo leakage after 12 h of incubation with serum proteins at 37 °C. *In vivo* pharmacokinetics studies using positron emission tomography showed a circulation half-life of 29.5 h and minimal accumulation in the liver and spleen. The demonstrated strategy, by incorporating unique protein tertiary structure in the headgroup of an amphiphile, opens new avenues to generate organic nanoparticles with tunable stability, ligand clustering, and controlled disassembly to meet current demands in nanomedicine.

KEYWORDS: 3-helix micelle · peptide–polymer conjugate · helix bundle · nanocarriers · stability

Effective micellar nanocarriers can improve the pharmacokinetics, biodistribution, toxicity profile, and efficacy of drug molecules and have been investigated extensively.[1−10] In order to maximize their therapeutic efficacy, micelle-based delivery systems should demonstrate (1) extended *in vivo* circulation half-life; (2) minimum cargo leakage during circulation; (3) controlled size for effective extravasations; and (4) degradation for eventual renal clearance to reduce systemic toxicity.

When administered intravenously, nanoscopic carriers offer the added advantage of concentrating in tumor tissues *via* the enhanced permeation and retention (EPR) effect defined by leaky vasculature and poor lymphatic drainage commonly seen in solid tumors.[11−14] The size of the nanocarrier is considered the most critical factor to fully take advantage of the EPR effect. The physiological factors, including the density and heterogeneity of the vasculature at the tumor site and interstitial fluid pressure, impact the extent of extravasation of nanocarriers into tumors. Current FDA-approved Doxil (~100 nm) and Abraxane (~130 nm) have provided only modest survival benefits presumably due to inefficient transport of the chemotherapeutic drug into the tumor.[15] Studies have shown that following extravasation into tumor interstitium, a drug or drug-encapsulated vehicle should be capable of travelling up to 100 μm away from the tumor vasculature in order to reach all cells within the tumor.[16] There is increasing evidence that a drug's limited penetration and distribution within a tumor, which results in insufficient elimination of malignant cells, may contribute to tumor repopulation after treatment.[17−20] Nanocarriers need to be below a certain size to achieve significant tumor penetration,[16,21] and the size cutoff value depends on the shape, hardness, and architecture of the carrier.[22,23] Recent studies using a 3D human melanoma xenograft model in mice showed that smaller particles (*i.e.*, 10−12 nm quantum dots) can more effectively penetrate the physiological barriers imposed by abnormal tumor vasculature and dense interstitial matrix than the 60 nm nanoparticles.[21] Using dendrimers, the physiologic upper limit of pore size in the blood–tumor barrier of malignant solid tumor

* Address correspondence to tingxu@berkeley.edu.

Received for review March 15, 2012 and accepted April 30, 2012.

Published online April 30, 2012
10.1021/nn301142r

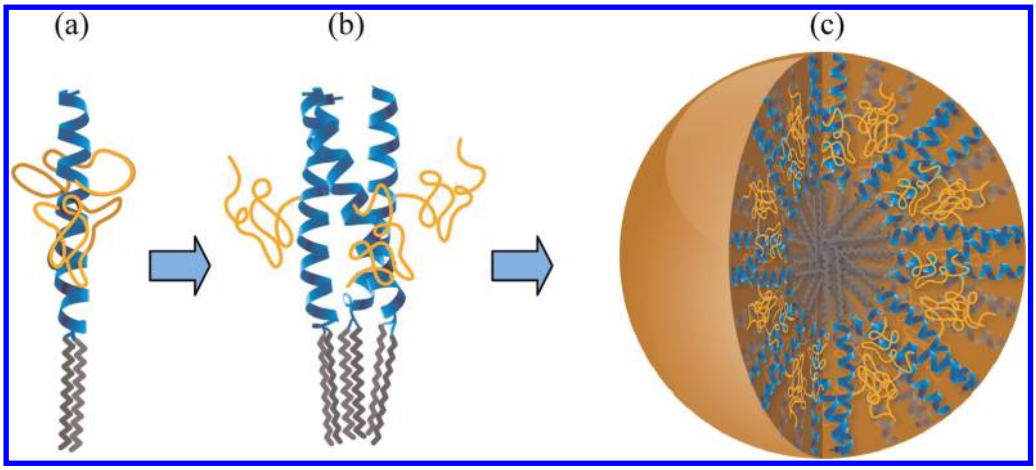

Scheme 1. (a) Schematic drawing of the designed amphiphile containing a short peptide helix with a polymer chain covalently linked to the side chain of the helix, hydrophobic tails attached to the N-terminus, and PEG or targeting ligands at the C-terminus. (b) Three amphiphiles associate to form a subunit, where the headgroup contains a 3-helix bundle with polymers covalently attached to the exterior. (c) Schematic drawing of the micelle, where the shell is composed of 3-helix bundles and the core is composed of aliphatic chains.

microvasculature is determined to be approximately 12 nm.[24] Organic nanoparticles based on elastin-like peptides, ~25 nm in size, demonstrated a nearly complete tumor regression in a murine cancer model.[25] There is a strong need to design and synthesize stable nanocarriers in the size range of 10–30 nm for potentially enhanced therapeutic efficacy.

The effectiveness of a drug carrier depends on its stability and drug retention *in vivo*. After systemic injections, the nanocarriers are confronted with dilution, as well as numerous components, such as proteins and cells, which can lead to cargo leakage. To ensure an improvement in the toxicity profile of the drug, the drug needs to be retained within micelles until reaching the target site. The kinetic stability of micelles determines the *in vivo* stability, circulation half-life, and clearance pathway.[26,27] As compared to covalent organic particles, micelles have very low intermolecular interactions among amphiphiles, typically a few kcal per mol. The subunit can exchange with local medium or among particles. The kinetic energy barrier of the exchange decreases as the micelle size reduces, especially when the size is below 20 nm. Small micelles are generally fluid, dynamic assemblies, where the subunit amphiphiles are constantly exchanging with the surrounding media and with other micelles. The presence of chemical traps *in vivo* that stabilize individual amphiphiles further reduces the stability of micelles and leads to undesirable cargo leakage and disassembly.[28–32]

In addition to the control on particle size and cargo stability, an equally important requirement for effective nanocarriers is the balance of long circulation and nanocarrier clearance.[33–35] Nanocarriers initially must be larger than 6 nm to achieve extended circulation lifetime and subsequently need to disintegrate into materials smaller than ~6 nm or 50 kDa in molecular weight to be eliminated from circulation by glomerular filtration in the kidney.[33] Chemically cross-linking the headgroups of an amphiphile and/or engineering multiple pairs of intermolecular interactions among the headgroups can be effective to obtain stable micelles. However, biodistribution studies indicated accumulation in the liver and spleen and raised concerns over the potential long-term toxicity.[36]

Taking all of the design criteria into consideration, it is highly desirable to generate micellar nanocarriers in the size range of 10–30 nm which combine a long circulation half-life, effective tumor tissue penetration, minimal cargo leakage, and efficient subunit clearance. To meet these requirements, we have synthesized small micelles by designing a new family of amphiphiles based on coiled-coil 3-helix bundle forming peptide–poly(ethylene glycol) conjugates. The designed amphiphiles form stable micelles, so-called "3-helix micelles", 15 nm in size. The 3-helix micelles demonstrated significantly enhanced stability in comparison to existing micelles in similar size range. Förster resonance energy transfer (FRET) studies showed minimal cargo leakage over 12 h in the presence of serum proteins at 37 °C. More importantly, *in vivo* pharmacokinetics studies using positron emission tomography (PET) showed a circulation half-life of 29.5 h. Additionally, the 3-helix micelle can be degraded and cleared with significantly reduced accumulation in the liver and spleen. These desirable attributes, including <20 nm particle size, long blood circulation, minimal cargo leakage, and efficient clearance, clearly validate the potential of 3-helix micelles as nanocarriers to meet current demands in nanomedicine.

RESULTS AND DISCUSSION

Amphiphilic Peptide–Polymer Design and Synthesis. The amphiphile is schematically shown in Scheme 1.

The headgroup is composed of a newly designed peptide–poly(ethylene glycol) (PEG) conjugate where the PEG chain is attached to the middle of a 3-helix bundle forming peptide (protein data bank code 1coi).[37,38] Structural studies and molecular dynamic simulation showed that the PEG chains locate in the exterior of the 3-helix bundle and stabilize the peptide's secondary and tertiary structures.[38,39] Two C18 alkyl chains were attached at the peptide N-terminus with a (6)-amino-hexanoic acid linker inserted between the peptide and the alkyl tail to introduce amphiphilicity. Another PEG chain is attached to the peptide C-terminus to provide a stealth layer in a similar fashion to that of PEGylated liposomes.[40,41] The resulting amphiphile is termed as "1coi-dC18-PEG2K". The intermolecular interactions between peptides and the compression of PEG on the exterior of the helix bundle increase the activation energy barrier for subunit desorption and provide stability to the micelle. Upon forming micelles, peptide–PEG conjugates in the headgroup will self-associate into a trimeric subunit (Scheme 1b) and may provide a platform to investigate the effect of the oligomeric state of ligand presentation on the active targeting for nanocarrier localization. The PEG chains attached to the exterior of the helix bundle may be used to tailor the interligand cluster distance.

The peptide 1coi (EVEALEKKVAALECKVQALEKKVEALEHGW) was synthesized using solid-phase peptide synthesis (SPPS). The synthetic methodology for the amphiphiles is shown in Figure 1. Specifically, the alkyl chains were conjugated on solid phase through reaction of stearic acids with deprotected Fmoc-Lys(Fmoc)-OH to generate a branched alkyl tail at the N-terminus. Orthogonal protection–deprotection strategies were employed to link PEG molecules on both the side and the C-terminus. The C-terminus was modified through palladium-catalyzed allyl deprotection of Fmoc-Lys(Alloc)-OH followed by conjugation of carboxy-terminated organic molecules using HBTU/DIPEA chemistry. In this study, PEG (M_w = 750 Da) was selected as the C-terminal functional group to generate a stealth layer to prevent nonspecific protein absorption. A variety of targeting ligands can also be attached using the same chemistry. The conjugate was purified by reverse-phase high-pressure liquid chromatography (RP-HPLC) using a gradient of mixed solvents containing water (0.1% TFA) and isopropyl alcohol (0.1% TFA). The amphiphilic molecules eluted at ~85% isopropyl alcohol with the overall yield of 30%. The molecular weight was confirmed by MALDI-TOF spectrometry (Figure 1).

Physical Characterization of Amphiphilic Micelles. The amphiphile 1coi-dC18-PEG2K spontaneously self-assembles into micelles above its CMC value (~2 μM) in aqueous solution. Figure 2a shows the circular dichroism (CD) spectrum of 200 μM solution of 1coi-dC18-PEG2K at 25 °C in phosphate buffer (pH = 7.4, 25 mM). There are two peaks with minima at 208 and 222 nm, typical of a highly α-helical structure. The 1coi peptide in the headgroup forms a helical structure with 82% helicity. The ratio of the molar ellipticities at 222 and 208 nm is routinely used to identify the presence of coiled-coil helices. For an isolated α-helix, the ratio was estimated to be 0.83,[42] while for interacting α-helices, such as coiled-coils, the ratio was calculated to be ~1.0.[43] The ratio between the ellipticities at 222 and 208 nm is 1.04, indicating that the tertiary structure of peptides, that is, the coiled-coil helix bundle, is maintained within micelles.

The packing parameter that quantifies the shape of amphiphiles was calculated using Israelachvili's surfactant number theory based on the size of the headgroup determined from X-ray and neutron scattering (unpublished results) and the crystal structure of 1coi. The packing parameter of a trimetric subunit, as shown in Scheme 1b, is calculated to be 0.238. For comparison, the packing parameter of individual amphiphiles, as schematically shown in Scheme 1a, is calculated to be 0.332. The formation of 3-helix bundles increased the cross-sectional mismatch between the headgroup and hydrophobic tails. On the basis of Israelachvili's surfactant number theory, the 3-helix bundle peptide–PEG conjugate has a strong preference for the formation of spherical micelles.[28] After dissolving the lyophilized amphiphile powder into buffered solution, dynamic light scattering (DLS) (Figure 2b) reveals a hydrodynamic diameter of 15 nm and a fairly uniform size distribution of micelles. Negatively stained TEM, as shown in Figure 2c, provided further evidence that the amphiphiles form spherical micelles with a diameter of ~15 nm.

Drug Loading. A range of hydrophobic drugs and dye molecules can be readily encapsulated in the micelles including doxorubicin (DOX), dipyrromethene boron difluoride (BODIPY), and lipophilic carbocyanines for fluorescence imaging. To evaluate the potential of the 3-helix micelles as nanocarriers for therapeutic applications, DOX was used to estimate the drug loading capacity. The encapsulation of DOX in the micelles was performed using a dry-down method. 1coi-dC18-PEG2K and DOX were first solubilized in methanol, dried, and rehydrated. After spin dialysis to remove free drugs, size exclusion chromatography (SEC) and DLS were used to characterize the homogeneity of the DOX-loaded micelles. As shown in Figure 3a, the overlapping elution profiles of the micelles monitored at 220 and 480 nm that monitor the peptide and DOX, respectively, verified the encapsulation of doxorubicin in the micelles and the absence of free drug. DLS experiments (Figure 3b) indicate that the addition of DOX did not disrupt the uniformity of the micelles, showing a single species with a diameter of 15 nm. Quenching of DOX fluorescence in micelles, compared to free DOX in solution, further confirmed the presence

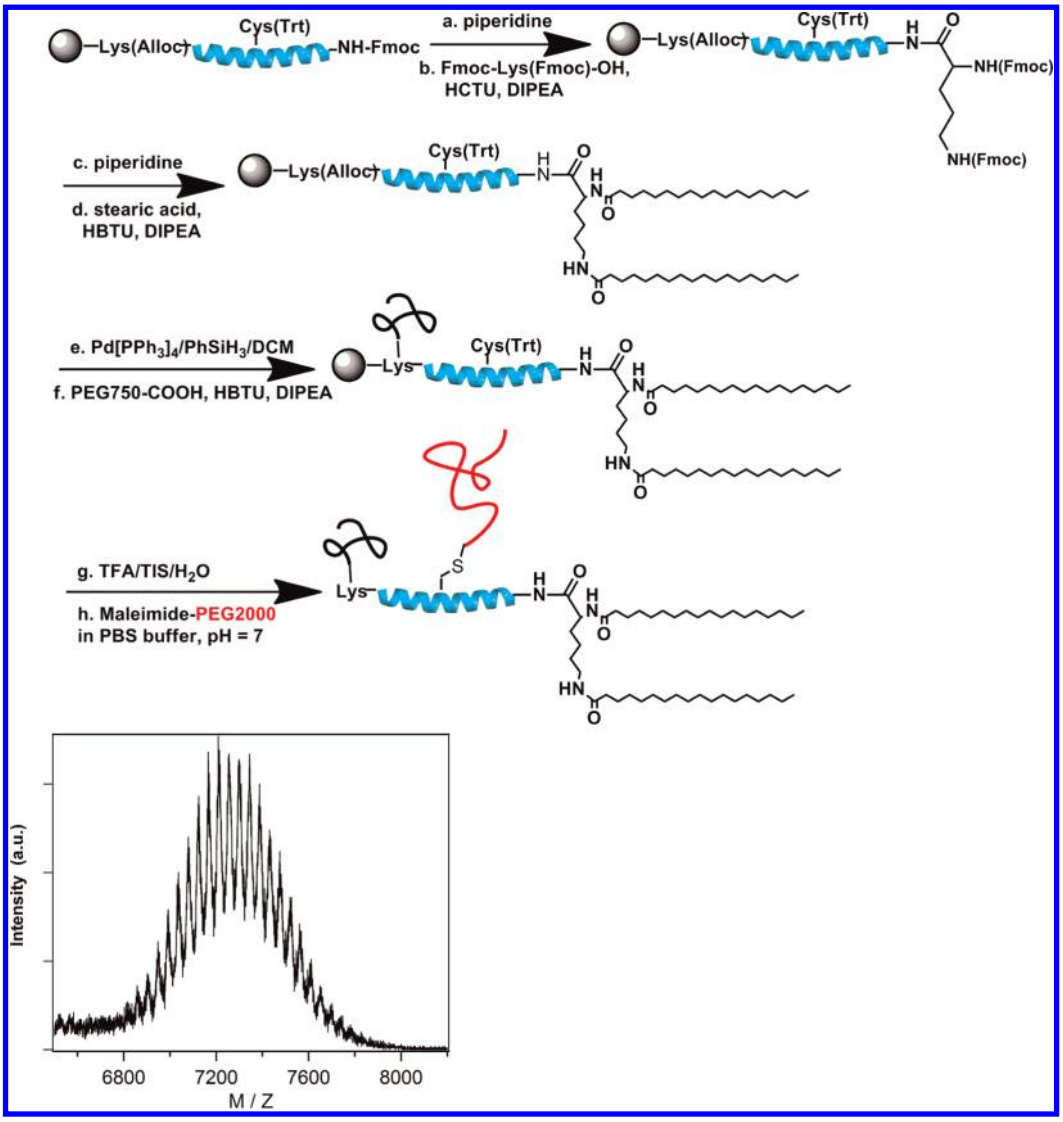

Figure 1. Synthetic scheme and MALDI spectrum of amphiphilic peptide−polymer conjugates. The postmodification of peptide 1coi was achieved through selective protection−deprotection strategy employed in Fmoc solid-phase peptide synthesis. Specifically, the alkyl chains were conjugated on solid phase through reaction of stearic acids with deprotected Fmoc-Lys(Fmoc)-OH to generate a branched alkyl tail. The C-terminus was modified through palladium-catalyzed allyl deprotection of Fmoc-Lys(Alloc)-OH followed by the conjugation of carboxy-terminated PEG (M_w = 750 Da) using HBTU/DIPEA chemistry. After TFA cleavage reaction, maleimide end-functionalized PEG2000 was appended in the middle of the peptide domain through site-specific Michael addition reaction. The conjugate was purified by reverse-phase high-pressure liquid chromatography (RP-HPLC) using a gradient of mixed solvents containing water (0.1% TFA) and isopropyl alcohol (0.1% TFA). The amphiphilic molecules were eluted at ~85% isopropyl alcohol. The overall purification yield is around 30%. The molecular weight was confirmed by MALDI-TOF spectrometry. The distance between neighboring peaks is 44 Da, corresponding to the mass of a PEG repeat unit.

of DOX in the micelles (Figure 3c). The DOX loading was determined by dissolving the lyophilized powder in methanol and monitoring the absorbance of the DOX at 480 nm. For both free DOX solution and DOX-encapsulated micelles, DOX concentration was the same based on UV absorbance at 480 nm. Thus, the fluorescence intensity shown in Figure 3c reflects the different local environment of DOX molecules. For DOX, drug loading in the range of 7−8 wt % was obtained reproducibly. This is comparable to the values obtained by covalent conjugation of DOX to dendrimers[44] and polypeptides,[25] where 4−10 wt % has been reported.

***In Vitro* Stability by FRET.** The entrapped drug must be maintained inside the carriers until reaching the target site; however, *in vivo* cargo leakage remains a long-standing issue for micellar nanocarriers. For dye-loaded block copolymer (BCP) micelles, *in vivo* FRET studies showed that dye molecules were released 15 min after intravenous injection.[45] The *in vitro* stability of the 3-helix micelles was evaluated using FRET in the presence of bovine serum albumin (BSA), which is known as an amphiphile trap that disrupts micellar nanocarriers.[31,46] A lipophilic FRET pair, 3,3′-dioctadecyloxacarbocyanine perchlorate (DiO, donor) and 1,1′-dioctadecyl-3,3,3′,3′-tetramethylindocarbocyanine perchlorate (DiI, acceptor),

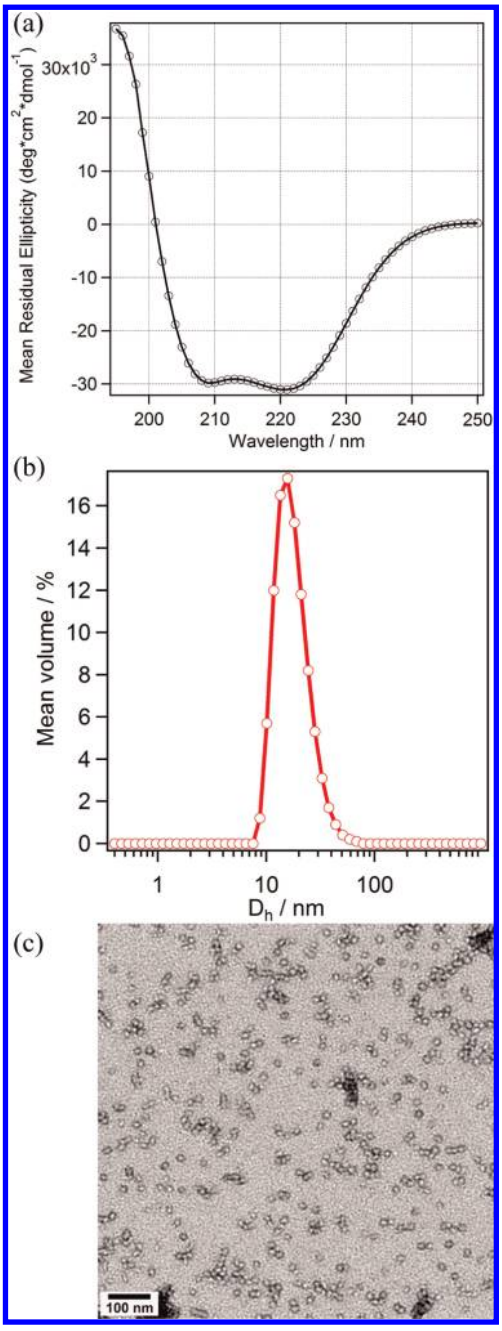

Figure 2. Physical characterization of micelles. (a) CD spectrum of 1coi-dC18-PEG2K (200 μM) for quantitative estimation of the secondary structure of the headgroup. (b) DLS measurement of 1coi-dC18-PEG2K micelles showing the size with an average diameter of 15 nm. (c) Negatively stained TEM of 1coi-dC18-PEG2K at 0.1 mg/mL in 25 mM phosphate buffer at pH 7.5, showing that individually dispersed spherical micelles are dominant.

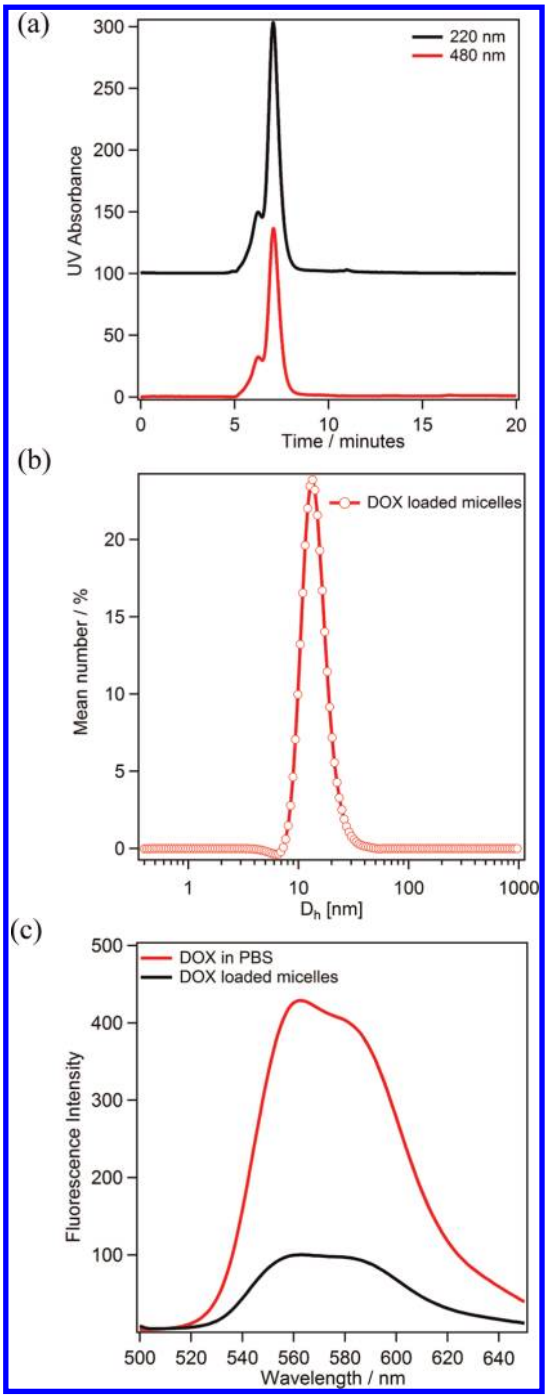

Figure 3. Structural characterization of DOX-loaded 1coi-dC18-PEG2K micelles. (a) SEC traces of DOX-loaded micelles monitored at 220 and 480 nm, showing a relative homogeneous morphology with minimal aggregation. (b) DLS of PEG750 surface-modified 1coi-dC18-PEG2K micelles with 8 wt % doxorubicin loading. The trace shows uniform particle size distribution with mean diameter of ~15 nm. (c) Fluorescence spectra of encapsulated DOX in micelles which showed much lower intensity compared to that of free DOX in solution.

were coencapsulated in 1coi-dC18-PEG2K micelles. As the control experiment, the same FRET dyes were coencapsulated in conventional micelles based on 1,2-distearoyl-*sn*-glycero-3-phosphoethanolamine-*N*-[methoxy(polyethylene glycol)-2000] (DSPE-PEG2K). Dye-encapsulated micelles were diluted in a physiological concentration of BSA (50 mg/mL) at 37 °C, and fluorescence was monitored in the range of 475−600 nm with λ_{ex} = 450 nm.

After initial equilibration in BSA (~10 min), a major emission peak is observed at 565 nm, which is accompanied by a minor emission peak at 505 nm. This indicates that both dyes are encapsulated within individual micelles and arranged in close proximity. If the

cargo molecules leach out, FRET turns "off" due to the increase in the intermolecular distance between DiO and DiI, resulting in a simultaneous increase of fluorescence intensity at 505 nm and decrease at 565 nm. For 1coi-dC18-PEG2K micelles, over time, the fluorescence intensity remains essentially unchanged at both 505 and 565 nm (Figure 4a). In contrast, for DSPE-PEG2K micelles, the intensity at 565 nm drops significantly, which is accompanied by an increase in fluorescence intensity at 505 nm (Figure 4b). The FRET ratio of $I_{565}/(I_{565} + I_{505})$ represents the efficiency of energy transfer and reflects the relative stability of micelles under the experimental conditions (Figure 4c).[30,45,47] A sharp decrease of the normalized FRET ratio is observed for DSPE-PEG2K micelles, indicating rapid cargo release out of micelles in BSA solution, whereas the ratio remains essentially constant for 3-helix micelles under the same conditions (Figure 4c). This result is consistent with previously reported results indicating that DSPE-PEG2K micelles have poor stability in BSA with a half-life of 20 min at 37 °C.[31]

***In Vivo* Studies of 3-Helix Micelles Using PET Imaging.** Pharmacokinetic evaluation and biodistribution of the 3-helix micelles were carried out to validate their potential as nanocarriers. The preparation of ^{64}Cu-labeled 3-helix micelles was achieved by co-assembly of metal-chelator-functionalized amphiphilic peptides with the regular amphiphilies followed by high affinity coordination reaction with ^{64}Cu ions. The detailed synthetic and labeling procedures are presented in the Supporting Information. Micelle solutions were administered through intravenous injection to mice bearing NDL tumors. Using positron emission tomography (PET), the pharmacokinetics of radiolabeled micelles was assessed and compared with long-circulating liposomes[48] and conventional DSPE-PEG2K micelles. All tested micelles have similar degrees of hydrophobicity, as they are composed of double C18 tails and a stealth layer of PEG to prevent nonspecific protein adsorption. PET images were acquired over 48 h after injection and demonstrated that the 3-helix micelles remained highly concentrated in the blood pool, with minimal liver and spleen accumulation (Figure 5a). Approximately 15 ± 1.5% ID/g remained circulating in the blood pool at 48 h post-injection (Figure 5b). The activity was confined to plasma rather than the circulating cellular components (Figure 5c). On the basis of the image data set, the pharmacokinetics of the 3-helix micelle was fitted using a biphase model. The β-phase blood circulation half-life ($t_{1/2,\beta}$) of the micelles was estimated to be ~29.5 h (Figure 5b), which is comparable to that of successful dendrimer−DOX conjugate showing a circulating half-life of 16 h and antitumor activity in a carcinoma model.[22,44] The half-life is in a range similar to those of polypeptide-based block copolymer micelles currently in clinical trials.[49]

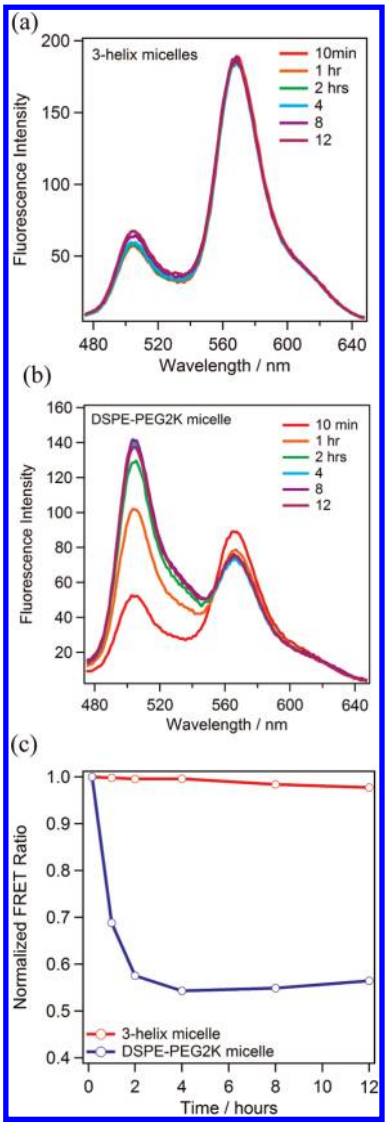

Figure 4. *In vitro* stability evaluation by time-resolved FRET in the presence of BSA at 37 °C. (a) 1coi-dC18-PEG2K micelles encapsulating DiO and DiI FRET pair dyes. (b) DSPE-PEG2K micelles encapsulating DiO and DiI FRET pair dyes. (c) Plot of normalized FRET ratio at each time point to time of 10 min *versus* time.

Figure 6 shows the comparison of the biodistribution profile of the 3-helix micelles with long-circulating liposomes and conventional DSPE-PEG2K-OMe micelles in nonperfused mice. The radioactivity resulting from injection of 3-helix micelles is the highest in the blood pool with 15.0 ± 1.5% ID/g. The uptake of the 3-helix micelles in NDL model tumors (5.7 ± 0.9% ID/g) was similar to that achieved with ^{64}Cu-liposomes (4.3% ID/g) and ^{64}Cu-albumin in a similar model (MIN-O) and may be attributed to the EPR effect.[50] The radioactivities of different organs are observed as follows: 4.6 ± 0.5% ID/g in the spleen, 4.5 ± 0.2% ID/g in the liver, 2.9 ± 0.3% ID/g in the kidney, 2.1 ± 0.2% ID/g in the heart. The animals were not perfused in our study. Considering that the high activity remained in blood at the point of the biodistribution study, the residual

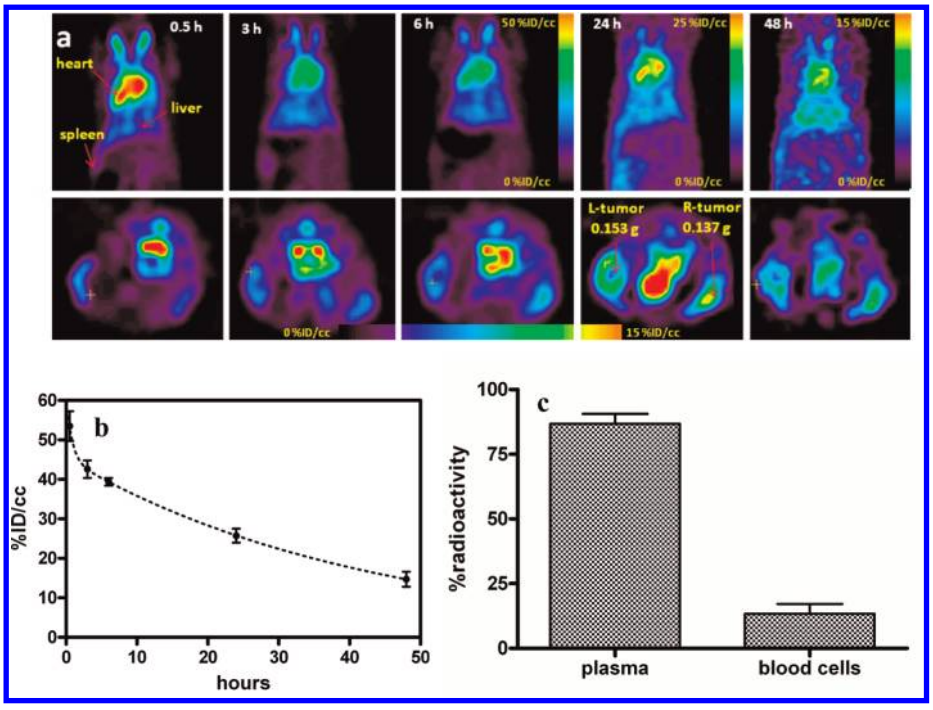

Figure 5. *In vivo* assessment of micelle circulation and stability. (a) Coronal (top) and transverse (bottom) view of sliced PET images of ^{64}Cu-1coi-dC18-PEG2k micelles administered in mouse. Images were acquired after the reconstruction of histogram with maximum a posteriori probability (MAP) estimate. (b) Blood radioactivity (%ID/cc) of ^{64}Cu-1coi-dC18-PEG2k micelles (n = 6) in blood. Curve was fitted as two-phase exponential decay ($Y = 45.32e^{-0.0235\times t} + 16.42e^{-1.27\times t}$, $t_{1/2}$ α = 0.55, β = 29.52). (c) Percent radioactivity of ^{64}Cu-1coi-dC18-PEG2k micelles (n = 4) in plasma and blood cells (48 h after injection). Percent radioactivity was calculated by the following eq [100 $\times$ plasma or blood cells radioactivity/(plasma radioactivity + blood cell radioactivity)].

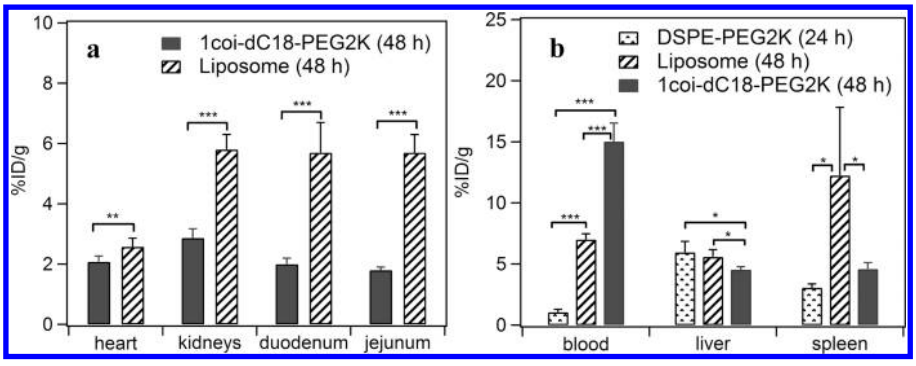

Figure 6. Biodistribution analysis (%ID/g) of conventional micelles (n = 2), ^{64}Cu-1coi-dC18-PEG2k micelles (n = 6), and long-circulating liposomes (n = 4). (a) Comparison of radioactivity (%ID/g) of long-circulating liposomes (liposomal 48 h data were obtained from a previous study[48]) and ^{64}Cu-1coi-dC18-PEG2k micelles (48 h). (b) Comparison of radioactivity (%ID/g) of conventional micelles, long-circulating liposomes (HSPC/cholesterol/DSPE-PEG2K-OMe = 56:39:5), and ^{64}Cu-1coi-dC18-PEG2K micelles. Statistical analysis between groups was performed with one-way ANOVA followed by Tukey's multiple comparison test (***P < 0.0001, **P < 0.001, *P < 0.05).

blood in liver and spleen may partially account for the activities observed in these organs. To further clarify the systemic clearance pathway, radioactivities in the duodenum and jejunum were measured, which are ~2% ID/g (Figure 6a). The low activity in the digestion system, liver, and spleen indicated that the reticulo-endothelial systems (RES) clearance may not be the primary clearance pathway for the 3-helix micelles.

The radioactivity detected within the blood, liver, and spleen was also compared among the 3-helix micelles, DSPE-PEG2K-OMe micelles, and long-circulating liposomes (Figure 6b). Due to the rapid clearance of DSPE-PEG2K-OMe micelles, biodistribution results at 24 h were used for comparison to those obtained at 48 h with long-circulating liposomes and 3-helix micelles. The radioactivity in the liver resulting from DPSE-PEG2K-OMe micelles remained at a similar level to that of long-circulating liposomes. Substantial differences between 3-helix micelles and long-circulating liposomes were apparent: blood circulation was extended, and liver and spleen accumulation was decreased compared with either previous strategy.

In vivo pharmacokinetics and biodistribution studies clearly demonstrated that 3-helix micelles achieved long circulation half-life and efficient clearance. We attribute the long circulation half-life to the micelle size, physical stability, and surface chemistry. Reduced accumulation in the liver, spleen, and intestine, combined with urinary activity, suggests that the 3-helix micelle was not primarily cleared through the RES pathway. One hypothesis for the systemic clearance of 3-helix micelles is first by monomer desorption, where individual or trimeric amphiphiles exit the micelle during blood circulation. If the hydrophobic C18 tails cannot be shielded by the headgroup, the amphiphiles will be captured by serum proteins and subsequently cleared by the RES system,[51] similar to results of other micelles, including DSPE-PEG2K and block-copolymer-based micelles. As the hydrophilic headgroup (*i.e.*, 1coi-PEG2K) is over 5 kDa in molecular weight, it is possible that 1coi-PEG2K may wrap the C18 chains to shield nonfavorable interactions between C18 and water. This is similar to our recent studies in 1coi–polystyrene conjugates where the 1coi unfolded and acted as a surfactant for the hydrophobic PS.[52] The molecular weight of the 1coi-dC18-PEG2K amphiphile is only ~6 kDa, well below the critical molecular weight cutoff to pass through the glomerular membranes. In the sequence of the 1coi peptide, there are a few sites that can be cleaved by proteases. As an alternative to physical desorption of micelles, the 3-helix micelles can be internalized into cells and digested *via* proteolysis. Once the peptide is enzymatically degraded, the micelle will disassemble and the fragments of the amphiphile will be metabolized.

CONCLUSIONS

In summary, we demonstrated a new design to prepare stable micelles based on amphiphilic 3-helix peptide–polymer conjugates. Our design is unique in two ways; that is, the helical peptide self-associates to form a common protein tertiary structure, coiled-coil helix bundle, and the PEG is covalently attached to the middle of the peptide helix and to the exterior of the helix bundle. The quantification of the energetic contributions from each component of the amphiphile is ongoing. However, our initial investigation suggests that it is the combination of these two factors that leads to exceptional stability of 3-helix micelles. Quantitative studies may open up a new avenue to generate organic nanoparticles with tunable stability, ligand clustering, and controlled disassembly and will be the focus of a later contribution. Present studies clearly demonstrate that these newly designed 3-helix micelles have many important attributes required for effective drug formulation that are not commonly seen for nanocarriers in this size range. Since each component of the amphiphile can be readily substituted, they also present numerous opportunities for other applications, such as nanocarriers with active targeting, vaccine formulation, delivery of peptide-based drugs, inhibitors and promoters, and nanoreactors for catalysis.

MATERIALS AND METHODS

The 1coi (EVEALEKKVAALECKVQALEKKVEALEHGW) is a *de novo* designed 3-helix bundle peptide and was synthesized on a Protein Technologies Prelude solid-phase synthesizer using standard 9-fluorenylmethyl carbamate (Fmoc) protection chemistry on PEG-PAL resin (Applied Biosystems), typically at 0.05 mmol scale. Fmoc-Lys(Fmoc)-OH (EMD Bioscience) was appended to the N-terminus to allow coupling of stearic acid molecules to the N-terminus of the peptide. To modify the C-terminus of the peptide with PEG750, Fmoc-Lys(Alloc)-OH was coupled at the C-terminus. The Alloc group was selectively removed by utilizing $Pd(PPh3)_4$ catalyst and radical trapping agent $PhSiH_3$ in DCM. The reaction was repeated five times. The resulting free amino groups of lysine were utilized for conjugating carboxy-terminated PEG750 using HBTU/DIPEA chemistry. The coupling reaction was performed at room temperature for 24 h and repeated twice. Peptides were then cleaved from the resin using standard procedures. Cysteine at position 14 facilitates the site-specific coupling of maleimide-functionalized PEG of molecular weight 2000 g/mol to the middle of the peptide sequence. Cysteine at the C-terminus of 1coi-dC18-PEG2K allows for the conjugation of 6-BAT-maleimide onto the peptides for PET imaging.

Negatively Stained Transmission Electron Microscopy. Lyophilized peptide powder was dissolved at 0.1 mg/mL in 25 mM phosphate buffer at pH 7.4. Five microliters of peptide solution was dropped on a discharged holey carbon coated grid (Ted Pella 01824). After removing excess peptide solution, 5 μL of phosphotungstic acid (2 wt %, pH = 3.3) solution was then applied for 2 min. Samples were dried in air and examined by a FEI Tecnai 12 transmission electron microscope at 120 kV.

Förster Resonance Energy Transfer (FRET). A lipophilic FRET pair, 3,3′-dioctadecyloxacarbocyanine perchlorate (DiO, donor) and 1,1′-dioctadecyl-3,3,3′,3′-tetramethylindocarbocyanine perchlorate (DiI, acceptor), were used to measure the energy transfer upon mixing. Desired amounts of DiO, DiI, and 1coi-dC18-PEG2K or DSPE-PEG2K were codissolved in a mixture of 1:1 chloroform and methanol. Organic solvents were evaporated under vacuum at 60 °C for at least 3 h to form a thin film in a glass vial. Phosphate buffer (pH = 7.4, 25 mM) was added to rehydrate the film at a concentration of 1 mg/mL. In cases where visible aggregates were formed, solution was heated in a water bath at 70 °C for at least 30 min to promote the homogeneity of the encapsulation. After 24 h stirring at room temperature, the solutions were then subject to centrifugation and spin dialysis to remove any insoluble aggregates and soluble dyes in the supernatant. To 350 μL of the BSA sample was added 10 μL of the dye-encapsulated micelle solution, and time-dependent fluorescence intensity was recorded in the range of 475 to 650 nm for 12 h with excitation wavelength at 450 nm.

MicroPET Imaging and Biodistribution Analyses. After the injection of ^{64}Cu-1coi-dC18-PEG2k micelles, female FVB mice (n = 6) bearing NDL tumors bilaterally within the mammary fat pads were imaged with microPET and the biodistribution was assessed. *In vivo* PET scans were obtained for 30 min immediately after tail vein injection of ^{64}Cu-1coi-dC18-PEG2k micelles

(11.7 ± 3.1 MBq and 86 ± 24 nmol lipid per mouse) in 150 μL of PBS and for 30 min at 3, 6, 24, and 48 h after injection. Animals anesthetized with 2−3% isoflurane were placed in pairs on the scanner bed, and PET acquisitions were obtained using a small animal PET scanner (Focus120, Siemens Medical Solutions, Inc.). After final time point scanning of each set of animals, animals were euthanized by cervical dislocation and blood was withdrawn by cardiac puncture. Briefly, once the animals were euthanized, organs were harvested for biodistribution and the radioactivity was measured in a γ-counter (Perkin-Elmer Life Sciences). For the biodistribution of ^{64}Cu-labeled conventional micelles, two female Balb/c mice weighing 26−27 g (Charles River, MA) were used. ^{64}Cu-labeled conventional micelles (7.33 ± 0.07 MBq and 69 ± 1 nmol lipids per mouse) were administered *via* the tail vein; the animals were sacrificed at 24 h after injection due to the rapid clearance of the radioactivity, and the procedures above were followed for biodistribution.

Conflict of Interest: The authors declare no competing financial interest.

Acknowledgment. H.D. was supported by Office of Army of the U.S. Department of Defense under contract W91NF-09-1-0374. J.Y.S., N.D., and T.X. were supported by the Office of Science, Office of Basic Energy Sciences, of the U.S. Department of Energy under contract DE-AC02-05CH11231. K.F., J.S., and L. M.M. were supported by NIH R01CA103828-6 and this publication has been funded in part with the Federal funds from the National Heart, Lung, and Blood Institute, National Institutes of Health, Department of Health and Human Services, under Contract No. HHSN268201000043C. Materials for drug encapsulation and biological studies are provided by the Li Ka Shing Woman Research Award.

Supporting Information Available: Additional experimental details. This material is available free of charge *via* the Internet at http://pubs.acs.org.

REFERENCES AND NOTES

1. Gref, R.; Minamitake, Y.; Peracchia, M. T.; Trubetskoy, V.; Torchilin, V.; Langer, R. Biodegradable Long-Circulating Polymeric Nanospheres. *Science* **1994**, *263*, 1600–1603.
2. Kirpotin, D.; Hong, K.; Park, J.; Colbern, G.; Shalaby, R.; Benz, C.; Papahadjopoulos, D. Design of Liposomes for Targeted Intracellular Delivery to Cancer Cells in Solid Tumors *in Vivo*. *FASEB J.* **1997**, *11*, A1425.
3. Kirpotin, D. B.; Park, J. W.; Hong, K.; Shao, Y.; Shalaby, R.; Colbern, C.; Benz, C. C.; Papahadjopoulos, D. Targeting of Liposomes to Solid Tumors: The Case of Sterically Stabilized Anti-Her2 Immunoliposomes. *J. Liposome Res.* **1997**, *7*, 391–417.
4. Papahadjopoulos, D.; Kirpotin, D. B.; Park, J. W.; Hong, K. L.; Shao, Y.; Shalaby, R.; Colbern, G.; Benz, C. C. Targeting of Drugs to Solid Tumors Using Anti-Her2 Immunoliposomes. *J. Liposome Res.* **1998**, *8*, 425–442.
5. Drummond, D. C.; Meyer, O.; Hong, K. L.; Kirpotin, D. B.; Papahadjopoulos, D. Optimizing Liposomes for Delivery of Chemotherapeutic Agents to Solid Tumors. *Pharmacol. Rev.* **1999**, *51*, 691–743.
6. Brannon-Peppas, L.; Blanchette, J. O. Nanoparticle and Targeted Systems for Cancer Therapy. *Adv. Drug Delivery Rev.* **2004**, *56*, 1649–1659.
7. Lee, C. C.; MacKay, J. A.; Fréchet, J. M. J.; Szoka, F. C. Designing Dendrimers for Biological Applications. *Nat. Biotechnol.* **2005**, *23*, 1517–1526.
8. Duncan, R. Polymer Conjugates as Anticancer Nanomedicines. *Nat. Rev. Cancer* **2006**, *6*, 688–701.
9. Sakarellos-Daitsiotis, M.; Krikorian, D.; Panou-Pomonis, E.; Sakarellos, C. Artificial Carriers: A Strategy for Constructing Antigenic/Immunogenic Conjugates. *Curr. Top. Med. Chem.* **2006**, *6*, 1715–1735.
10. Hubbell, J. A.; Thomas, S. N.; Swartz, M. A. Materials Engineering for Immunomodulation. *Nature* **2009**, *462*, 449–460.
11. Maeda, H.; Matsumura, Y.; Sasamoto, K. Tumor Targeting Mechanism by Biocompatible Macromolecular Drugs. *Proc. Am. Assoc. Cancer Res.* **1986**, *27*, 401.
12. Matsumura, Y.; Maeda, H. A New Concept for Macromolecular Therapeutics in Cancer Chemotherapy: Mechanism of Tumoritropic Accumulation of Proteins and the Antitumor Agent Smancs. *Cancer Res.* **1986**, *46*, 6387–6392.
13. Jan, E, S. Caveolae: From Basic Trafficking Mechanisms to Targeting Transcytosis for Tissue-Specific Drug and Gene Delivery *in Vivo*. *Adv. Drug Delivery Rev.* **2001**, *49*, 265–280.
14. Torchilin, V. P. Recent Advances with Liposomes as Pharmaceutical Carriers. *Nat. Rev. Drug Discovery* **2005**, *4*, 145–160.
15. Gabizon, A. A.; Shmeeda, H.; Zalipsky, S. Pros and Cons of the Liposome Platform in Cancer Drug Targeting. *J. Liposome Res.* **2006**, *16*, 175–183.
16. Minchinton, A. I.; Tannock, I. F. Drug Penetration in Solid Tumours. *Nat. Rev. Cancer* **2006**, *6*, 583–592.
17. Tunggal, J. K.; Ballinger, J. R.; Tannock, I. F. Influence of Cell Concentration in Limiting the Therapeutic Benefit of P-Glycoprotein Reversal Agents. *Int. J. Cancer* **1999**, *81*, 741–747.
18. Tunggal, J. K.; Cowan, D. S. M.; Shaikh, H.; Tannock, I. F. Penetration of Anticancer Drugs through Solid Tissue: A Factor That Limits the Effectiveness of Chemotherapy for Solid Tumors. *Clin. Cancer Res.* **1999**, *5*, 1583–1586.
19. Tannock, I. F.; Lee, C. M.; Tunggal, J. K.; Cowan, D. S. M.; Egorin, M. J. Limited Penetration of Anticancer Drugs through Tumor Tissue: A Potential Cause of Resistance of Solid Tumors to Chemotherapy. *Clin. Cancer Res.* **2002**, *8*, 878–884.
20. Primeau, A. J.; Rendon, A.; Hedley, D.; Lilge, L.; Tannock, I. F. The Distribution of the Anticancer Drug Doxorubicin in Relation to Blood Vessels in Solid Tumors. *Clin. Cancer Res.* **2005**, *11*, 8782–8788.
21. Popovic, Z.; Liu, W. H.; Chauhan, V. P.; Lee, J.; Wong, C.; Greytak, A. B.; Insin, N.; Nocera, D. G.; Fukumura, D.; Jain, R. K.; *et al.* A Nanoparticle Size Series for *In Vivo* Fluorescence Imaging. *Angew. Chem., Int. Ed.* **2010**, *49*, 8649–8652.
22. Fox, M. E.; Szoka, F. C.; Fréchet, J. M. J. Soluble Polymer Carriers for the Treatment of Cancer: The Importance of Molecular Architecture. *Acc. Chem. Res.* **2009**, *42*, 1141–1151.
23. Nasongkla, N.; Chen, B.; Macaraeg, N.; Fox, M. E.; Fréchet, J. M. J.; Szoka, F. C. Dependence of Pharmacokinetics and Biodistribution on Polymer Architecture: Effect of Cyclic *versus* Linear Polymers. *J. Am. Chem. Soc.* **2009**, *131*, 3842–3843.
24. Sarin, H.; Kanevsky, A. S.; Wu, H. T.; Sousa, A. A.; Wilson, C. M.; Aronova, M. A.; Griffiths, G. L.; Leapman, R. D.; Vo, H. Q. Physiologic Upper Limit of Pore Size in the Blood-Tumor Barrier of Malignant Solid Tumors. *J. Transl. Med.* **2009**, *7*, 51.
25. Andrew MacKay, J.; Chen, M.; McDaniel, J. R.; Liu, W.; Simnick, A. J.; Chilkoti, A. Self-Assembling Chimeric Polypeptide-Doxorubicin Conjugate Nanoparticles That Abolish Tumours after a Single Injection. *Nat. Mater.* **2009**, *8*, 993–999.
26. Batrakova, E. V.; Li, S.; Li, Y.; Alakhov, V. Y.; Elmquist, W. F.; Kabanov, A. V. Distribution Kinetics of a Micelle-Forming Block Copolymer Pluronic P85. *J. Controlled Release* **2004**, *100*, 389–397.
27. Liu, J.; Zeng, F.; Allen, C. *In Vivo* Fate of Unimers and Micelles of a Poly(ethylene glycol)-Block-Poly(caprolactone) Copolymer in Mice Following Intravenous Administration. *Eur. J. Pharm. Biopharm.* **2007**, *65*, 309–319.
28. Israelachvili, J. N.; Mitchell, D. J.; Ninham, B. W. Theory of Self-Assembly of Hydrocarbon Amphiphiles into Micelles and Bilayers. *J. Chem. Soc., Faraday Trans.* **1976**, *72*, 1525–1568.
29. Castelletto, V.; Krysmann, M.; Kelarakis, A.; Jauregi, P. Complex Formation of Bovine Serum Albumin with a Poly(ethylene glycol) Lipid Conjugate. *Biomacromolecules* **2007**, *8*, 2244–2249.

30. Chen, H. T.; Kim, S. W.; Li, L.; Wang, S. Y.; Park, K.; Cheng, J. X. Release of Hydrophobic Molecules from Polymer Micelles into Cell Membranes Revealed by Forster Resonance Energy Transfer Imaging. *Proc. Natl. Acad. Sci. U.S.A.* **2008**, *105*, 6596–6601.
31. Kastantin, M.; Missirlis, D.; Black, M.; Ananthanarayanan, B.; Peters, D.; Tirrell, M. Thermodynamic and Kinetic Stability of DSPE-PEG(2000) Micelles in the Presence of Bovine Serum Albumin. *J. Phys. Chem. B* **2010**, *114*, 12632–12640.
32. Nicolai, T.; Colombani, O.; Chassenieux, C. Dynamic Polymeric Micelles *versus* Frozen Nanoparticles Formed by Block Copolymers. *Soft Matter* **2010**, *6*, 3111–3118.
33. Choi, H. S.; Liu, W.; Misra, P.; Tanaka, E.; Zimmer, J. P.; Ipe, B. I.; Bawendi, M. G.; Frangioni, J. V. Renal Clearance of Quantum Dots. *Nat. Biotechnol.* **2007**, *25*, 1165–1170.
34. Choi, H. S.; Ashitate, Y.; Lee, J. H.; Kim, S. H.; Matsui, A.; Insin, N.; Bawendi, M. G.; Semmler-Behnke, M.; Frangioni, J. V.; *et al.* Rapid Translocation of Nanoparticles from the Lung Airspaces to the Body. *Nat. Biotechnol.* **2010**, *28*, 1300–1303.
35. Choi, H. S.; Liu, W.; Liu, F.; Nasr, K.; Misra, P.; Bawendi, M. G.; Frangioni, J. V. Design Considerations for Tumour-Targeted Nanoparticles. *Nat. Nanotechnol.* **2010**, *5*, 42–47.
36. Sun, X.; Rossin, R.; Turner, J. L.; Becker, M. L.; Joralemon, M. J.; Welch, M. J.; Wooley, K. L. An Assessment of the Effects of Shell Cross-Linked Nanoparticle Size, Core Composition, and Surface PEGylation on *In Vivo* Biodistribution. *Biomacromolecules* **2005**, *6*, 2541–2554.
37. Ogihara, N. L. W.; Manfred, S.; Degrado, W. F. Crystal Structure of the Designed Trimeric Coiled Coil Coil-Vald: Implications for Engineering Crystals and Supramolecular Assemblies. *Protein Sci.* **1997**, *6*, 80–88.
38. Shu, J. Y.; Tan, C.; DeGrado, W. F.; Xu, T. New Design of Helix Bundle Peptide−Polymer Conjugates. *Biomacromolecules* **2008**, *9*, 2111–2117.
39. Jain, A.; Ashbaugh, H. S. Helix Stabilization of Poly(ethylene glycol)−Peptide Conjugates. *Biomacromolecules* **2011**, *12*, 2729–2734.
40. Papahadjopoulos, D.; Allen, T. M.; Gabizon, A.; Mayhew, E.; Matthay, K.; Huang, S. K.; Lee, K. D.; Woodle, M. C.; Lasic, D. D.; Redemann, C. Sterically Stabilized Liposomes: Improvements in Pharmacokinetics and Antitumor Therapeutic Efficacy. *Proc. Natl. Acad. Sci. U.S.A.* **1991**, *88*, 11460–11464.
41. Drummond, D. C.; Meyer, O.; Hong, K.; Kirpotin, D. B.; Papahadjopoulos, D. Optimizing Liposomes for Delivery of Chemotherapeutic Agents to Solid Tumors. *Pharmacol. Rev.* **1999**, *51*, 691–744.
42. Zhou, N. E.; Kay, C. M.; Hodges, R. S. Synthetic Model Proteins. Positional Effects of Interchain Hydrophobic Interactions on Stability of Two-Stranded Alpha-Helical Coiled-Coils. *J. Biol. Chem.* **1992**, *267*, 2664–2670.
43. Choy, N.; Raussens, V.; Narayanaswami, V. Inter-molecular Coiled-Coil Formation in Human Apolipoprotein E C-Terminal Domain. *J. Mol. Biol.* **2003**, *334*, 527–539.
44. Lee, C. C.; Gillies, E. R.; Fox, M. E.; Guillaudeu, S. J.; Fréchet, J. M. J.; Dy, E. E.; Szoka, F. C. A Single Dose of Doxorubicin-Functionalized Bow-Tie Dendrimer Cures Mice Bearing C-26 Colon Carcinomas. *Proc. Natl. Acad. Sci. U.S.A.* **2006**, *103*, 16649–16654.
45. Chen, H.; Kim, S.; He, W.; Wang, H.; Low, P. S.; Park, K.; Cheng, J. X. Fast Release of Lipophilic Agents from Circulating PEG-PDLLA Micelles Revealed by *In Vivo* Forster Resonance Energy Transfer Imaging. *Langmuir* **2008**, *24*, 5213–5217.
46. Missirlis, D.; Khant, H.; Tirrell, M. Mechanisms of Peptide Amphiphile Internalization by Sjsa-1 Cells *in Vitro*. *Biochemistry* **2009**, *48*, 3304–3314.
47. Jiwpanich, S.; Ryu, J.-H.; Bickerton, S.; Thayumanavan, S. Noncovalent Encapsulation Stabilities in Supramolecular Nanoassemblies. *J. Am. Chem. Soc.* **2010**, *132*, 10683–10685.
48. Seo, J. W.; Zhang, H.; Kukis, D. L.; Meares, C. F.; Ferrara, K. W. A Novel Method To Label Preformed Liposomes with ^{64}Cu for Positron Emission Tomography (PET) Imaging. *Bioconjugate Chem.* **2008**, *19*, 2577–2584.
49. Matsumura, Y. Poly(amino acid) Micelle Nanocarriers in Preclinical and Clinical Studies. *Adv. Drug Delivery Rev.* **2008**, *60*, 899–914.
50. Rygh, C. B.; Qin, S.; Seo, J. W.; Mahakian, L. M.; Zhang, H.; Adamson, R.; Chen, J. Q.; Borowsky, A. D.; Cardiffaa, R. D.; Reed, R. K.; *et al.* Longitudinal Investigation of Permeability and Distribution of Macromolecules in Mouse Malignant Transformation Using PET. *Clin. Cancer Res.* **2011**, *17*, 550–559.
51. Semple, S. C.; Chonn, A.; Cullis, P. R. Interactions of Liposomes and Lipid-Based Carrier Systems with Blood Proteins: Relation to Clearance Behaviour *in Vivo*. *Adv. Drug Delivery Rev.* **1998**, *32*, 3–17.
52. Shu, J. Y.; Huang, Y.-J.; Tan, C.; Presley, A. D.; Chang, J.; Xu, T. Amphiphilic Peptide−Polymer Conjugates Based on the Coiled-Coil Helix Bundle. *Biomacromolecules* **2010**, *11*, 1443–1452.